Title

Energy absorption and propagation in laser-created sparks

Journal

Applied Spectroscopy, 58(6)

ISSN

0003-7028

Authors

Bindhu, C V
Harilal, S S
Tillack, M S
et al.

Publication Date

2004-06-01

Peer reviewed

Energy Absorption and Propagation in Laser-Created Sparks

C. V. BINDHU, S. S. HARILAL,* M. S. TILLACK, F. NAJMABADI, and A. C. GAERIS

Center for Energy Research, University of California San Diego, 9500 Gilman Drive, La Jolla, California 92093-0438

The energy absorption and laser propagation characteristics of air and argon sparks at one atmosphere have been investigated. To create the sparks, 532 nm pulses from a frequency doubled Q-switched Nd:YAG laser are used. We employed 2 ns gated fast photography for studying the time evolution of the kernel at early times. Optical emission spectroscopy is used to infer temperature and density of the sparks. Significant energy absorption by the plasma is observed just above the breakdown threshold. The energy absorption and propagation in the spark indicated that argon plasma is more absorptive than air plasma. The absorption of the spark increases with laser energy, and at higher energies absorption saturation is observed. A spiky behavior is observed in the transmitted temporal profiles of lasers at higher energies and this is explained as due to the formation of a self-regulating regime.

Index Headings: **Laser-induced gas breakdown; Emission spectroscopy; Laser propagation; Energy absorption; Spark photography.**

INTRODUCTION

When a powerful focused laser beam interacts with a gaseous medium, a spark is created.[1,2] This high-pressure region develops a shock wave into the ambient medium that has sufficient strength to ignite a gaseous mixture[3] or to extinguish a diffusion flame.[4] Laser-induced gaseous plasmas can be used for a variety of applications including elemental analysis,[5,6] detecting airborne biological agents,[7] quantitative analysis of aerosols,[8] production of X-rays and soft X-rays,[9,10] ultra fast shutters,[11] etc. Gas breakdown studies represent the initial step in research in inertial confinement fusion (ICF) and plasma heating by laser radiation. Different authors have examined the shapes and expansion of the laser-induced breakdown kernels using fast photography,[12] Schlieren photography,[13] and laser-induced fluorescence techniques.[14] The temporal, spatial, and spectral features of a plasma kernel suggest that it can be used as a pulsed bright and broadband ultraviolet-visible light source.[15]

The ionization of a gas in the presence of an electromagnetic field takes place by different mechanisms such as multiphoton absorption, cascade ionization via inverse bremsstrahlung, etc.[16,17] Both of these phenomena are treated theoretically by different groups.[18,19] In intense light an electron can gain sufficient energy by absorbing photons from the radiation field in collision with neutral atoms to produce ionization. If the laser irradiance is high enough, the multiphoton ionization process can generate the initial electrons from which an electron cascade can develop. Breakdown will occur if the electron density can reach a critical value despite losses due to diffusion, electron attachment, etc. A more detailed account of breakdown threshold calculations was given by Kroll and Watson,[18] in which they review existing literature on various loss processes of importance for breakdown such as diffusion, attachment, and vibrational and electronic excitation. Inverse bremsstrahlung is dominant when the product of gas pressure and pulse width $P\tau > 10^{-7}$ torr s. For smaller values of $P\tau$, collisions do not have time to occur during the laser pulse and multiphoton ionization is regarded as the dominant mechanism for creating a spark.

Most of the experiments related to laser-induced gas breakdown studies have centered largely on the measurements of breakdown threshold, while a little effort has been made on studies of energy absorption and propagation in a spark.[20–22] Recently, Chen et al.[12] reported laser-induced breakdown and energy deposition in air at atmospheric pressure using the fundamental frequency from a Q-switched Nd:YAG laser. Their results give quantitative guidance for the selection of the laser energy to achieve the desired breakdown probability and energy deposition characteristics of the plasma. The present investigation is designed to study the interaction of a focused laser pulse with one atmosphere air or argon and subsequent energy propagation through the spark medium. We analyzed how much energy can be propagated through a spark medium and how the spark affects the temporal profiles of the laser. The optical breakdown is created by focusing 532 nm, 8 ns pulses from a frequency doubled Q-switched Nd:YAG laser. Fast photography is undertaken to evaluate the evolution of the plasma kernel at earlier times. Spectroscopic methods are used for elucidating temperature and density of the sparks.

EXPERIMENTAL SETUP

The experimental arrangement used for the creation of laser sparks and studies of beam propagation is shown in Fig. 1. We used pulses from a frequency doubled Q-switched Nd:YAG laser (full width at half-maximum, FWHM, 8 ns) for creating breakdown plasma. The laser pulse parameters were monitored using a photodiode, a beam profiler (Photon Inc.), and a CLAS 2D wavefront sensor (Wavefront Sciences). The pulses were temporally cleaned up by the Quanta Ray injection seeder attachment. The spatial structure of the laser profile was approximately Gaussian. The pulse energy was varied by using a combination of wave plate and cube beam splitter.

To create breakdown plasma, the laser pulses were focused using an *f*/5 antireflection-coated laser aplanat (CVI Laser, LAP 75.0–15.0) having a focal length of 75 mm.

Received 23 September 2003; accepted 2 February 2004.

* Author to whom correspondence should be sent. E-mail: harilal@fusion.ucsd.edu.

0003-7028/04/5806-719$2.00/0

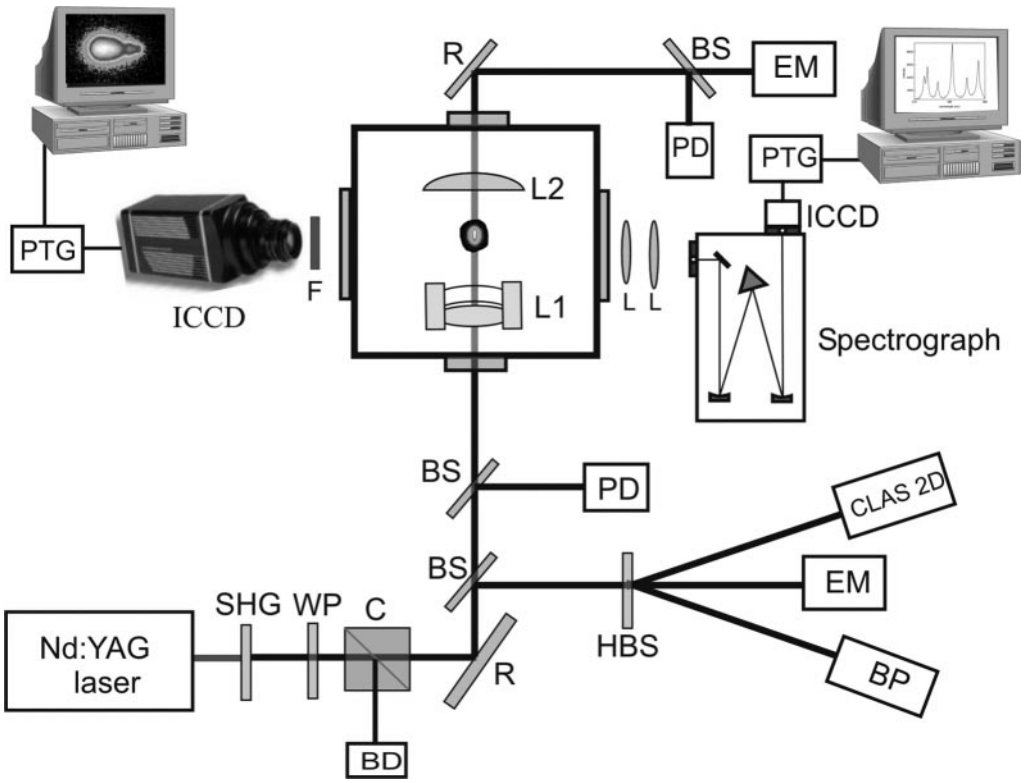

FIG. 1. The schematic of the experimental setup used for imaging, spectroscopy, propagation, and energy absorption studies. (SHG) Second-harmonic generator; (WP) wave plate; (C) cube beam splitter; (BD) beam dump; (R) reflector; (BS) beam sampler; (F) 532 nm filter; (ICCD) intensified charge-coupled device; (PTG) programmable timing generator; (L1) high-energy laser aplanat; (L2) lens; (HBS) holographic beam sampler; (EM) energy meter; (BP) beam profiler; (CLAS2D) CLAS2D Shack Hartman sensor; and (PD) photo diode.

A 75 mm antireflection-coated plano-convex lens was used for collimating the laser beam after passing through the focal region. The optical elements were placed in a vacuum chamber.

Photodiodes (Electro-optics Technology, Model EOT 2000, rise time: 200 ps) and energy/power meters (Ophir) were used to record temporal profiles and energy of each incoming and transmitted laser pulse through the focal volume. The temporal profiles were monitored using a 1 GHz Digital Phosphor Oscilloscope (Tektronix TDS5014, 5 GS/s maximum real-time sample rate).

The kernel imaging was accomplished using an intensified charge-coupled device (ICCD, PI MAX, Model 512 RB) placed orthogonal to the laser propagation direction. A Nikon lens was used to image the plume region onto the camera to form a two-dimensional image of the plume intensity. In order to eliminate 532 nm stray photons reaching the camera, a magenta subtractive filter was used. A programmable timing generator was used to control the delay time between the laser pulse and the imaging system with overall temporal resolution of 1 ns.

For emission spectroscopic studies, an optical system was used to image the spark onto the entrance slit of a 0.5-m spectrograph (Acton Pro, Spectra-Pro 500i), so as to have one-to-one correspondence with the sampled area of the spark and the image. The spectrograph was equipped with a tri-grating turret (150, 600, and 2400 grooves/mm) and an ICCD camera that was operated with vertical binning to obtain spectral intensities versus wavelength.

RESULTS AND DISCUSSION

The breakdown threshold is one of the first parameters of interest in characterizing the formation of plasma in a gaseous medium. When a lens focuses the laser beam, the distribution of irradiance in the focal spot is determined by the mode structure in the laser oscillator, by the effect of amplifiers and apertures in the system, and by the parameters of the lens. Single-element lenses were used in most of the previous experiments[12,14,20,22–26] for focusing high-power laser beams and significant spherical aberration was often present, though it may be minimized by a suitable choice of curvatures. The presence of aberrations may lead to erroneous values of optical breakdown threshold even when the measured spot size is used for the determination.[27] The effect of spherical aberration on the distribution of irradiance in the focal region has been calculated by Evans and Morgan.[28] In order to avoid or minimize spherical aberration, we used a two-element laser aplanat for focusing the laser beam. As a rule of thumb, a lens should be considered perfect or diffraction limited if the optical path difference (OPD) is less than ¼ wave. The estimated OPD of the laser aplanat used in the present studies using Zemax image analysis[29] is about $\frac{1}{5}$ wave, so the aberration effects are expected to be insignificant.

The breakdown threshold is determined by observing the initiation of the plasma kernel using the ICCD camera and looking at the absorption in the transmitted laser pulse through the focal volume. The measured break-

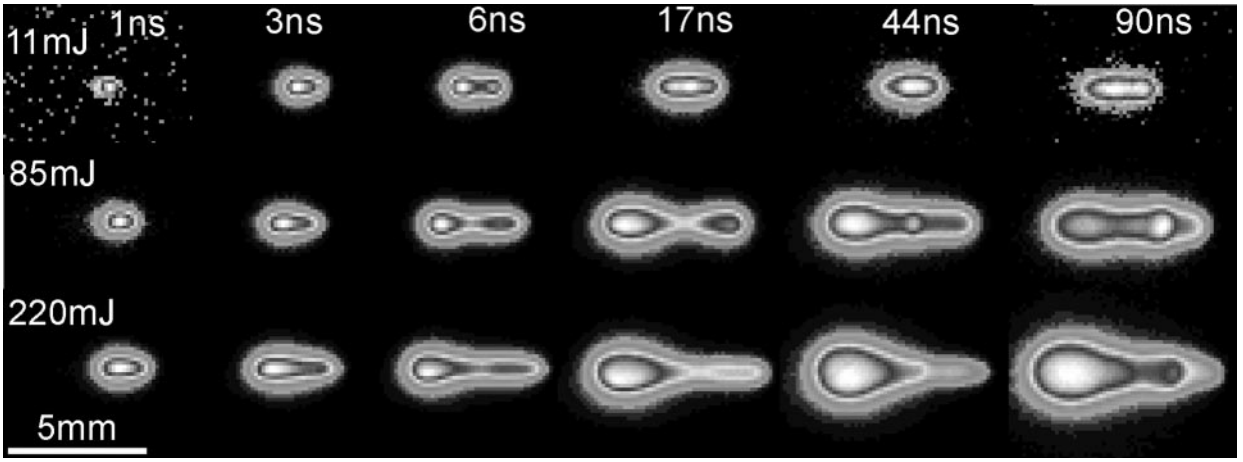

FIG. 2. The time evolution of visible emission from an air spark at different laser energies recorded using an ICCD camera. The exposure time used was 2 ns. The timings in the images represent the time after the onset of plasma formation. All of the images are normalized to their maximum intensity. The laser is coming from the left-hand side. The time sequence of each row is given along the top and the energy used for creating each column is given along the left side.

down threshold for air and argon at 1 atmosphere is $(2.5 \pm 0.2) \times 10^{12}$ W cm^{-2} and $(2.3 \pm 0.2) \times 10^{12}$ W cm^{-2}, respectively. The focal spot dimensions ($\sim$6 μm) used in determining the threshold irradiances quoted here are not measured directly but are calculated from the beam divergence (measured using a CLAS 2D Shack Hartmann sensor) and the focal spot estimated using Zemax image analysis. It is difficult to compare breakdown thresholds directly from the literature as experimental parameters rarely match. The breakdown threshold value of air is in good agreement with that previously reported by Phuoc[22] with almost identical experimental conditions.

Spark Imaging. The time evolution of the spark kernel is studied using fast photography and the shapes of the breakdown kernel observed show interesting behavior. Figures 2 and 3 give the time evolution of air and argon sparks at 1 atmosphere at different energy levels. The duration of the intensification (exposure time) is 2 ns and each image in the figure is recorded from an independent breakdown event. The laser beam is incident from the left-hand side. It should be remembered that each image given in the figures is spectrally integrated in the region 350–900 nm due to emission from the excited states of various species. They are not necessarily representative of the total flux because a part of the plume is nonluminous.[30,31] For better clarity, all of the images are normalized to their maximum intensity. This gives a fast on-scale overview of the data.

The shapes of the air spark (Fig. 2) at early times and at low energies are spherical and are confined very close to the focal volume. But as time elapses the spherical shape is changed to an elliptical shape. With increasing laser energy, the kernel becomes more asymmetrical in shape; the backward-moving plasma (towards the focusing lens) grows much faster than the forward-moving plasma (away from the focusing lens). The subsequent radiation expansion of the hot plasma leaves a rarefied region in the focal volume. The initiation time is earlier and the rate of growth is faster if the pulse energy is increased. The layer of gas outside the plasma, although it is transparent to the laser beam, is heated by the plasma radiation. This outside gas close to the plasma will in turn be ionized to such an extent that it will strongly absorb the laser light. This layer will then be further heated very rapidly and the temperature increases. By this time a new layer of plasma nearer the laser will have become strongly absorbing, so the boundary of the plasma will move towards the focusing lens. The absorption of the laser photons by the plasma is mainly due to the inverse bremsstrahlung process, which is so dominant that it leads to the development of a laser-supported radiation wave that propagates toward the laser beam. The time scale of this event is that of the laser pulse itself. The time evolution of the laser-created argon spark (Fig. 3) at different energy levels showed remarkable differences in comparison with the air spark. At low energy levels (near the breakdown threshold), the behavior of the argon spark resembled the air spark. But as the energy of the pulse increases, the forward-moving spark component is totally absent. After the initial breakdown, the plasma is heated to a point where it is opaque to the incoming laser beam. The optically thick plasma absorbs practically all the incident radiation after breakdown. We used the imaging data to create position–time (R–t) plots and the velocities of the sparks moving towards the focusing lens are measured from the slopes of the R–t graph. The estimated velocity of spark propagation towards the laser beam is given in Fig. 4 for air and argon for different laser energies. From the figure it is evident that the velocity of the spark front increases with laser energy.

In the present studies, the incident laser irradiance used is clearly greater than 1 GWcm^{-2} and for those cases for which the absorbed energy significantly exceeds the breakdown threshold, the plasma propagates as a laser-supported radiation wave. For a laser-supported radiation wave, the velocity is given by[32] $v = I/\rho E$, where I is the incident laser intensity, ρ is the mass density of the gas, and E is the internal energy. As the mass density of the air at 1 atm (1.205×10^{-3} g/mL) is smaller than the density of argon at 1 atm (1.664×10^{-3} g/mL), it is expected that a laser-supported radiation wave in air will propagate faster than one in argon. This is also supported by the fact that the ratio of the velocities of air and argon

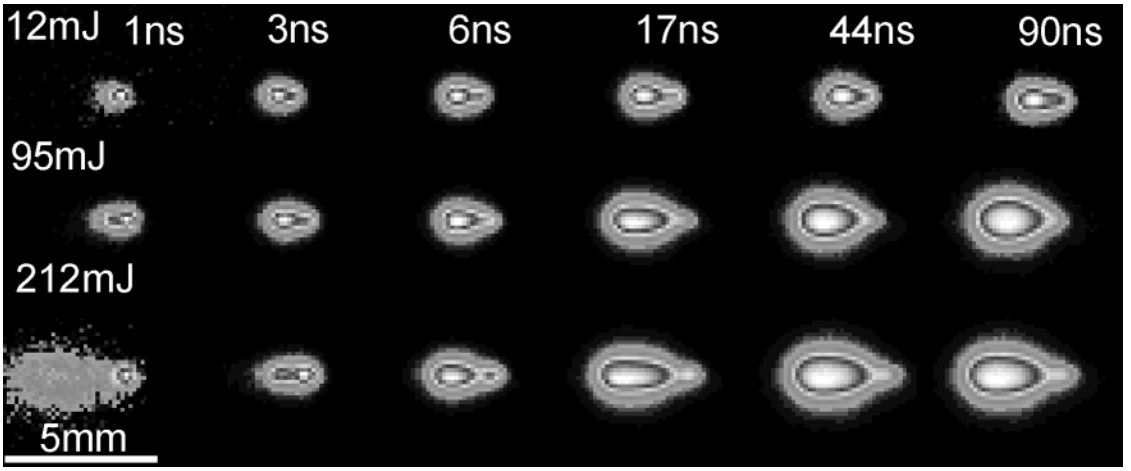

FIG. 3. ICCD photographs of the time evolution of visible emission from a laser-produced argon spark at different laser energies. The experimental parameters are the same as described in Fig. 2. All of the images are normalized to their maximum intensity.

sparks at a particular laser energy matches well with the ratio of their mass densities. The scaling law for the propagation velocity of the laser-supported radiation wave is:[32]

$$v \propto I^{4/(\beta+4)} \tag{1}$$

where β is a constant whose value varies between 1.5 and 1.6 for most ionized gases. A fit with the above equation is also given in Fig. 4, which is in good agreement at higher laser energies.

In air and argon sparks, a cascade-like growth of ionization is evident. The electron cascade requires the existence of initial electrons. The electrons then absorb more photons via the inverse bremsstrahlung process. A cascade growth of electron energy and the absorption coefficient of the plasma will be greatly influenced by the nature of the gas used. The condition necessary for the cascade-like growth is given by:[32]

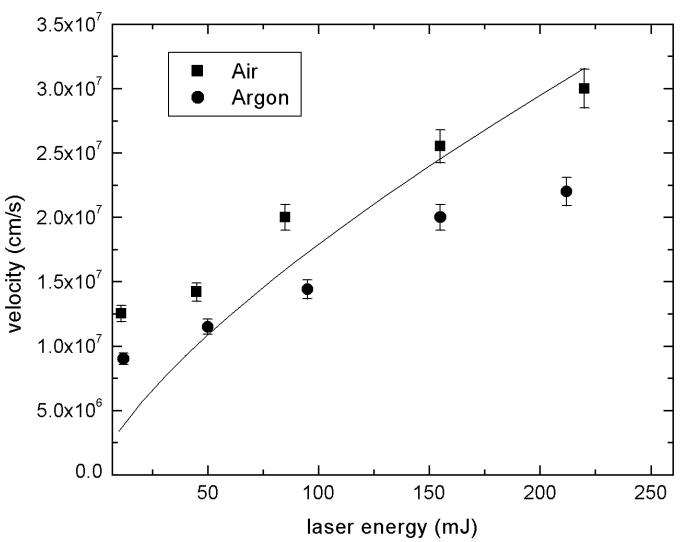

FIG. 4. The estimated velocity of the spark propagation towards the laser beam with laser energy for argon and air sparks showing that the air spark is moving faster than the argon spark. The solid curve in the plot represents the propagation velocity calculated from the scaling law of the laser-supported radiation wave.

$$\frac{d\varepsilon}{dt} = \frac{4\pi^2 e^2 I \nu_{\text{eff}}}{n_e c \omega^2} - \frac{2 m_e \nu_{\text{eff}} E}{M} > 0 \tag{2}$$

where ε is the energy of the free electrons; e and m_e are the charge and mass of the electron; M is the mass of the background gas neutral particle; E is the energy of the first ionization state of the gas; ν_{eff} is the effective frequency of electron neutral collision; n_e is electron density; I is the radiation intensity; and ω is the cyclic frequency of radiation. The first term on the right-hand side represents the rate of growth of energy by the absorption of laser photons and the second term gives the maximum rate of energy loss due to elastic and inelastic collisions with neutral gas particles. In comparing argon and air atmospheres, cascade growth is more favored for argon (M = 40 and E = 15.75 eV) in comparison with air (for nitrogen, M = 14 and E = 14.54 eV). So the spark formed in argon is more absorptive than that formed in air. This is also supported by the fact that the forward component of the kernel is absent for the argon spark.

The expansion of the spark continues even after the end of laser pulse, though much more slowly. The time evolution of the spark at later times showed dissipation times of ~5 ms.[33] It was noticed that the shape of the sparks changes significantly at later times.[33,34]

Spectroscopic Studies. For the study of absorption behavior of the laser-created sparks, the fundamental spark parameters are necessary. In order to determine the density and temperature of the sparks, spectroscopic methods are used.[17,35,36] The plasma electron temperature was deduced from the Boltzmann plot method and for its determination it was necessary to assume that the sparks produced are in local thermodynamic equilibrium (LTE). Several N^+ and Ar^+ lines were selected in order to calculate electron temperatures of air and argon sparks, respectively. The designation and other spectroscopic constants used for determination of the excitation temperature for air and argon sparks by the Boltzmann plot method are shown in Table I. Transition probabilities (A_{ij}) and statistical weights (g) of these lines are obtained from the literature.[37,38] The plasma electron density was measured using Stark broadened profiles of singly charged ions in the spark. For the air spark, the stark broadening of N^+

TABLE I. Spectroscopic data of N^+ and Ar^+ employed for temperature determination.

	Wavelength (nm)	Energy (eV) (upper level)	g (upper level)	Transition probability A_{ij} (10^8 s^{-1})
N^+	399.5	21.60	5	1.35
	444.7	23.20	5	1.14
	463.0	21.16	5	0.772
	504.5	20.90	3	0.342
	567.9	20.66	7	0.525
	594.1	23.25	7	0.554
Ar^+	385.1	19.97	4	0.387
	392.6	24.28	4	1.4
	404.3	21.40	4	0.406
	407.2	21.50	6	0.58
	410.4	22.70	4	1.3
	472.7	19.76	4	0.588
	476.5	19.87	4	0.64
	480.6	19.22	6	0.78
	484.8	19.30	2	0.849

at the 463.05 nm line and for the argon spark the Ar^+ line at 480.6 nm are selected. The impact parameters of these lines are obtained from Griem.[38]

The air and argon spark temperature and density as a function of axial position and laser energy are given in Figs. 5 and 6, respectively. The inset in Fig. 5 shows the designation of the radial positions. The focal point is chosen as the 0 position. For these studies time-integrated intensities were used and the temperature value presented should be regarded as indicative of the average conditions occurring in the spark, rather than defining the conditions at a particular stage of its evolution. In general, at an axial position, the temperature of the spark is not much influenced by the laser energy. With increasing laser energy the spark propagates towards the laser beam. The temperature of the air and argon sparks showed somewhat the same tendency. The sparks become much hotter

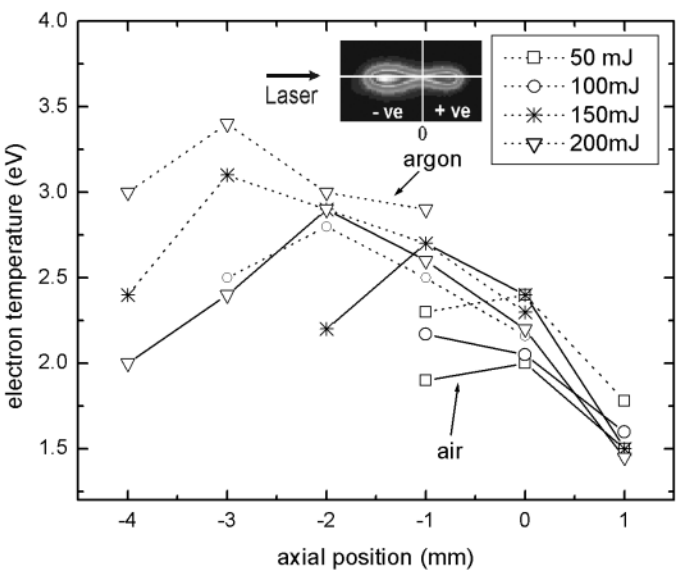

FIG. 5. The temperature of the spark at different axial positions in the spark for varying laser energies. As shown in the inset, the position 0 corresponds to the focal point and the −ve axis represents the co-ordinate towards the focusing lens. The data points with solid lines correspond to the air spark and those with dashed lines correspond to the argon spark.

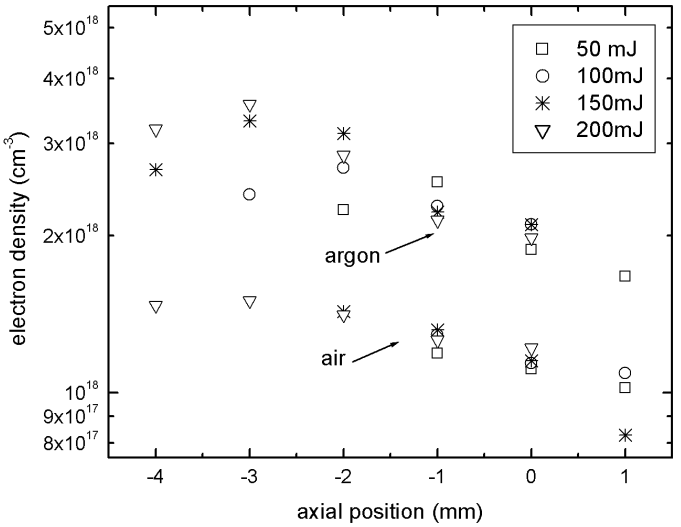

FIG. 6. The measured electron density at different axial points. The position 0 corresponds to the focal point and the −ve axis represents the co-ordinate towards the focusing lens.

with spatial positions towards the focusing lens, especially at higher energies.

The density estimates of the argon and air sparks are shown in Fig. 6. From the figure it is clear that at a given spatial position and laser energy, the density of the argon spark is much higher compared to the air spark. This will directly affect the absorption process of the spark. In the present studies, the absorption of the laser photons by the spark is mainly expected due to the inverse bremsstrahlung process. The inverse bremsstrahlung absorption via free electrons is approximated by:[39,40]

$$\alpha_{ib} = 1.37 \times 10^{-35}\, \lambda^3 n_e^2 T_e^{-1/2} \qquad (3)$$

where λ is the wavelength of the laser in μm. The absorption due to inverse bremsstrahlung calculated for air and argon sparks at different energy levels are given in Fig. 7. The inverse bremsstrahlung absorption depth es-

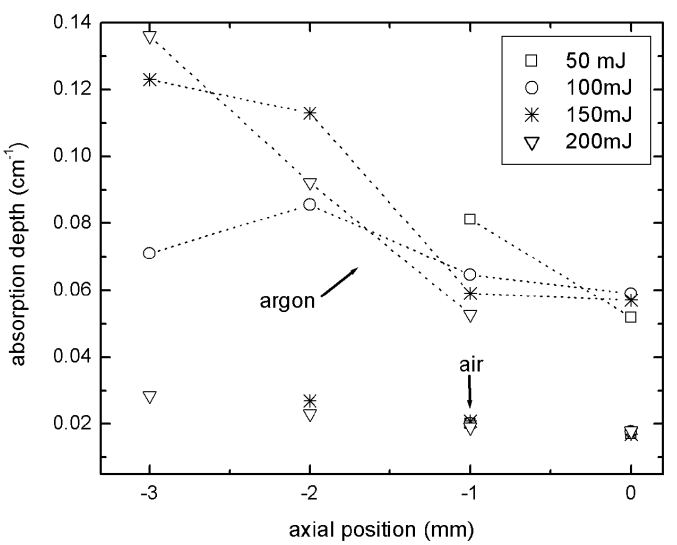

FIG. 7. The estimated inverse bremsstrahlung absorption depth for argon and air sparks for different laser energies. The data points without lines represent the air spark while data points with dashed curves represent the argon spark.

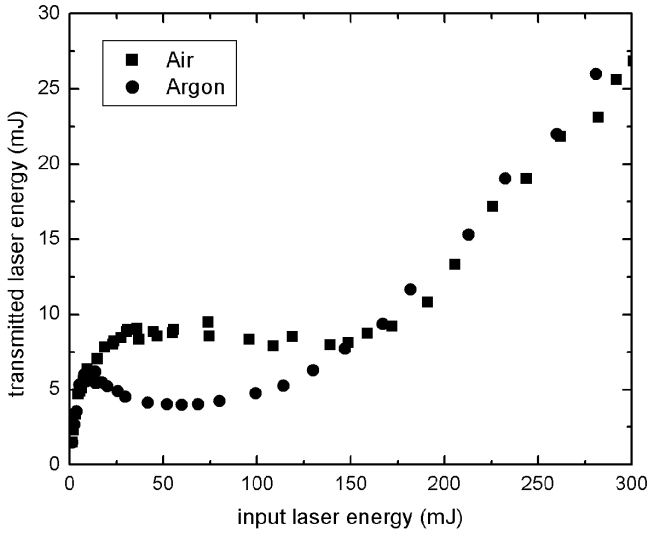

FIG. 8. Plot of transmitted laser energy after passing through the focal volume with respect to the incident laser energy.

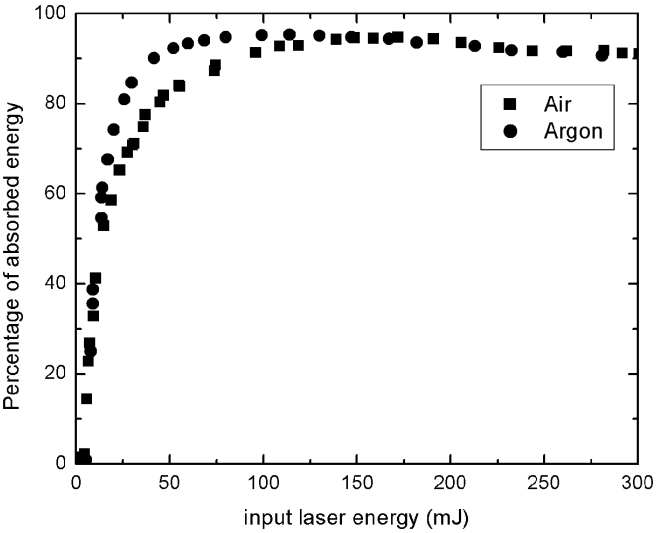

FIG. 9. The percentage of absorbed and scattered laser energy by the air and argon sparks obtained from Fig. 8 plotted against incident laser energy.

timation also showed that the argon spark is much absorptive than the air spark.

Propagation and Energy Absorption. In the previous section, we discussed the behavior of the breakdown kernel with time and laser pulse energy for air and argon. In this section, the attenuation of the laser beam passing through the focal volume is discussed. Figures 8 and 9 give energy propagation and absorption by the laser spark in air and argon at 1 atmosphere pressure. All the data points are corrected for reflection losses by different optical elements used in the experiment. The attenuation of the transmitted laser energy in the presence of breakdown is expected to be due to absorption, reflection, and scatter of the laser light by the spark plasma. The reflection of the incident photons by the spark depends on the plasma frequency ν_p, which should be lower than the laser frequency. For the Nd:YAG laser, its second-harmonic wavelength corresponds to a frequency of $\nu_l = 5.6 \times 10^{14}$ Hz. The plasma frequency is given by $\nu_p = 8.9 \times 10^3 n_e^{0.5}$. The estimated electron density calculated using Stark broadening at earlier times for air and argon sparks is $\sim 10^{19}$ cm^{-3}, which corresponds to $\nu_p = 2.8 \times 10^{13}$ Hz, which is much smaller than the laser frequency. So the energy losses due to reflection of the laser photons by the plasma can be assumed to be insignificant. Since significant scattering is not observed in the experiment, attenuation of the transmitted laser energy can be considered to be due solely to absorption by the spark.

When breakdown occurs in a dense gas, the attenuation of laser light passing through the focal volume increases abruptly, which implies that following the initiation of breakdown the free electrons grow to a highly absorbent density within a short period of time. For stronger laser excitation, the electron growth rate is expected to be much faster than the reciprocal of the laser pulse width.[12] As the laser energy increases well above the breakdown threshold, most of the energy (>80%) is absorbed by the spark (Fig. 9) and a small fraction is transmitted. The transmitted energy is more or less constant for the air spark when the input pulse energy varies between 30 to 150 mJ. For argon, the transmitted energy decreases with increasing energy immediately after breakdown. When we increase the laser energy after the breakdown, the percentage of absorbed energy increases much more quickly for argon than for air. At still higher energies, the transmitted energy starts to increase gradually with respect to incident energy. This may be caused by saturation of plasma absorption. Saturation of laser-produced plasma parameters has been observed and reported in the measurements of the number density of free electrons, electron temperature, etc.[41] When more energy is deposited into the plasma, the induced plasma tends to expand its size instead of becoming hotter and denser.

In order to obtain better insight into energy absorption, we examined the temporal profiles of the transmitted laser pulse through the spark. Figures 10 and 11 give the normalized temporal profiles of the laser pulse at different laser energies after propagating through the focal vol-

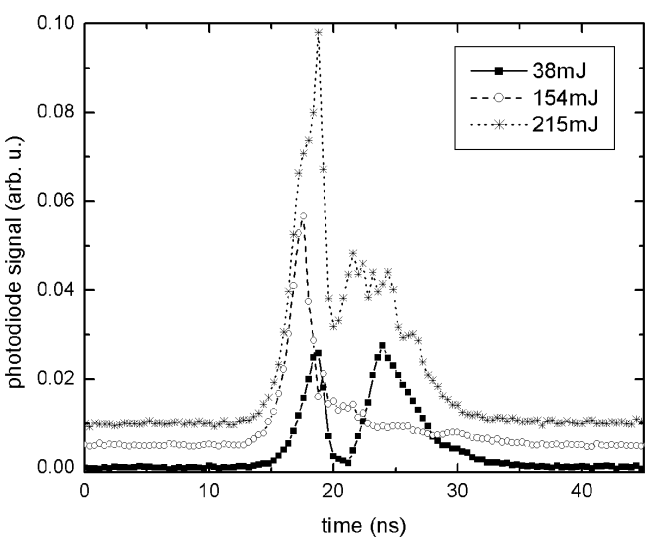

FIG. 10. The temporal structure of the transmitted laser pulse through the air spark recorded at different input laser energies. The baselines of all but the lowest energy are offset in order to be shown in a single plot.

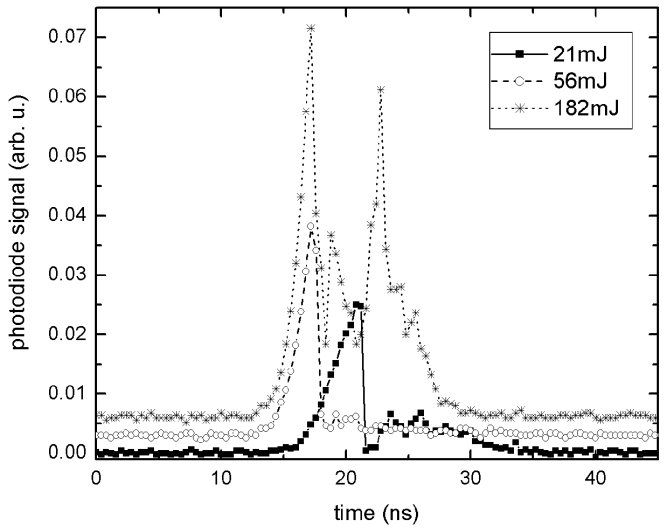

FIG. 11. The temporal profiles of the transmitted laser pulse after passing through the argon spark at different input energy levels. The baselines of all but the lowest energy are offset in order to be shown in a single plot.

ume in air and argon sparks. At low energies—before the onset of plasma formation—no change in the temporal profile is observed. But as energy increases, which leads to optical breakdown, the temporal shape of the transmitted laser pulse changes dramatically. The starting point of breakdown also varied in time with laser energy. Since the energy absorption process begins only when the laser energy exceeds the breakdown threshold value, the leading edge of the pulse below the threshold is transmitted unperturbed into and through the focal region. Our measurements showed that when the laser pulse energy is at the threshold of breakdown, there exits an uncertainty in the percentage of absorption, and temporal profiles show large variation. This sporadic behavior is due to the difficulty of generating initial electrons at the breakdown threshold values. But when the laser energy is well above the breakdown threshold, the transmitted temporal profiles are steady. All of the temporal profiles given in Figs. 10 and 11 are recorded using laser energy well above the breakdown threshold value and are easily reproducible.

In air, the spark absorbs energy immediately after the breakdown and a dip appears in the temporal profile of the transmitted laser pulse (Fig. 10). Since the plasma formation has a negative contribution to the refractive index, this leads to defocusing of the trailing edge of the laser pulse that is transmitted through the spark. As energy increases, a laser-supported radiation wave forms and the spark begins to absorb more energy after the breakdown event. This is evidenced by the fact that the dip as well as the width of the temporal profile increases with laser energy. At higher energies, the spark becomes opaque to the laser pulse and absorbs almost all the energy after breakdown. At 150 mJ the pulse is shortened to 2 ns and only the leading edge is transmitted. At still higher energies ($>$160 mJ), the spark again begins to transmit the trailing edge of the laser pulse.

Figure 11 demonstrates the way in which the transmitted temporal profiles develop with laser energy for an argon spark. Even at low energies, the argon spark absorbs almost all the energy after the breakdown event and the transmitted pulse is shortened to 2 ns (FWHM). With increasing energy, the breakdown starts earlier and the transmitted pulse becomes more and more narrow. At still higher energies, as shown in Fig. 11, the spark begins to transmit a part of the trailing edge. A spiky behavior in the temporal profiles of the transmitted pulse is observed at higher energies.

Both air and argon sparks transmit the trailing edge of the laser pulse at higher energies. The plot of transmitted laser energy with respect to incident laser energy (Fig. 8) also showed an increase in transmittance at higher energies for both air and argon sparks. Two main mechanisms can contribute to the increased transmittance of laser energy at high input energy levels: self-focusing and absorption saturation. Strong electromagnetic radiation applied to a spark causes redistribution of electrons and ions. This electron motion continues until the gas dynamic pressure balances the forces exerted on the plasma by the laser field. This leads to a decrease of the electron concentration and hence increases of the refractive index on the beam axis, which may lead to self-focusing. But, self-focusing is not evident with 2 ns gated images of sparks. Another plausible mechanism is absorption saturation at higher energies. At higher energies, apart from increased transmittance, the transmitted temporal pulse shows a spiking nature for both air and argon sparks. At high energy levels, when the spark absorbs an appreciable amount of energy, a self-regulating regime may form. If the absorption of the laser photons by the spark saturates, then the laser photons are transmitted through the spark. But with time, as the spark expands, the density and temperature decrease. This consequently increases the absorption of the laser photons by the spark, which in turn decreases the transmitted photons. This process continues until the end of the laser pulse. Similar self-regulating properties were observed and reported with laser-produced plasmas from solid targets.[41,42]

CONCLUSION

The laser propagation and energy absorption in air and argon sparks at 1 atmosphere pressure have been investigated. The laser-induced spark is created by focusing 8 ns pulses from a frequency doubled Nd:YAG laser. The spatial and temporal behavior of laser sparks was investigated using 2 ns fast photography. Significant energy absorption and cascade-type optical breakdown starts with the generation of initial free electrons. Following the rapid growth of electron density, the initial plasma becomes optically thick and absorbs nearly all of the incident energy in the latter portion of the laser pulse. Because of this, soon after the breakdown an apparent shift of the spark results from the build up of a laser-supported radiation wave that travels against the incoming laser beam, whereas the opposite side, obscured by the absorbing plasma, is no longer fed by the laser energy. The observed movement towards the laser beam ceases by the end of the laser pulse; at this stage emission intensity reaches the maximum value, from which it decays in time. The spark developed in air propagates not only backward but also forward, which differed from the spark

produced in argon, which showed only backward movement.

The laser propagation and energy absorption studies showed that spark absorption starts immediately after breakdown and more than 50% of the laser energy is absorbed just above the optical breakdown. The significant energy absorption by the plasma above the breakdown threshold indicates that inverse bremsstrahlung is important in subsequent heating and ionization of the plasma. With increasing laser energy, the absorption depth is found to be higher for argon than for air, indicating that cascade-like growth is more favored in argon. The measurements of the electron density of the sparks also showed that argon sparks are much denser than air sparks. The investigation of spark images using fast photography along with emission spectroscopy and energy absorption studies gives much insight into the laser–matter and laser–plasma interaction. The studies also indicate that for elemental analysis the energy of the pump laser should be kept just above the breakdown threshold. With increasing laser energy above the breakdown threshold the size of the spark increases rather than its temperature and density because of the spark absorption.

The transmitted temporal profiles showed large variation in absorption at the breakdown threshold region. But the temporal profiles become steady just above the breakdown threshold. At low energies a trailing part of the laser pulse is transmitted for an air spark, while an argon spark absorbs all radiation after the breakdown event. The transmittance of the trailing edge of the pulse is caused by defocusing of the laser pulse by the plasma. At higher energies the transmitted energy increases with incident energy and shows spiky behavior in the transmitted pulse. The increased transmittance at higher energies may be caused by absorption saturation. The spiky behavior in the transmitted temporal profiles at higher energies is explained by the formation of a self-regulating regime.

1. F. Martin, R. Mawassi, F. Vidal, I. Gallimberti, D. Comtois, H. Pepin, J. C. Kieffer, and H. P. Mercure, Appl. Spectrosc. **56,** 1444 (2002).
2. C. Aragon and J. A. Aguilera, Appl. Spectrosc. **51,** 1632 (1997).
3. T. X. Phuoc and F. P. White, Combust. Flame **119,** 203 (1999).
4. R. W. Schmieder, J. Appl. Phys. **52,** 3000 (1981).
5. R. J. Nordstrom, Appl. Spectrosc. **49,** 1490 (1995).
6. L. Dudragne, P. Adam, and J. Amouroux, Appl. Spectrosc. **52,** 1321 (1998).
7. J. D. Hybl, G. A. Lithgow, and S. G. Buckley, Appl. Spectrosc. **57,** 1207 (2003).
8. D. W. Hahn and M. M. Lunden, Aerosol Sci. Technol. **33,** 30 (2000).
9. H. Fiedorowicz, A. Bartnik, H. Szczurek, H. Daido, N. Sakaya, V. Kmetik, Y. Kato, M. Suzuki, M. Matsumura, J. Tajima, T. Nakayama, and T. Wilhein, Opt. Commun. **163,** 103 (1999).
10. R. Doron, E. Behar, P. Mandelbaum, J. L. Schwob, H. Fiedorowicz, A. Bartnik, R. Jarocki, M. Szczurek, and T. Wilhein, Phys. Rev. A **59,** 188 (1999).
11. L. J. Dhareshwar, P. A. Naik, and D. D. Bhawalkar, Rev. Sci. Instrum. **62,** 369 (1991).
12. Y. L. Chen, J. W. L. Lewis, and C. Parigger, J. Quant. Spectrosc. Radiat. Transfer **67,** 91 (2000).
13. A. J. Alcock, Phys. Rev. Lett. **20,** 1095 (1968).
14. Y. L. Chen and J. W. L. Lewis, Opt. Exp. **9,** 360 (2001).
15. A. Borghese and S. S. Merola, Appl. Opt. **37,** 3977 (1998).
16. G. V. Ostrovska and A. N. Zaidel, Sov. Phys. Usp. **16,** 834 (1974).
17. T. P. Hughes, *Plasmas and Laser Light* (John Wiley and Sons, New York, 1975).
18. N. Kroll and K. Watson, Phys. Rev. A **5,** 1883 (1972).
19. C. G. Morgan, Rep. Prog. Phys. **38,** 621 (1975).
20. B. K. Deka, P. E. Dyer, D. J. James, and S. A. Ramsden, Opt. Commun. **19,** 292 (1976).
21. I. C. E. Turcu, M. C. Gower, and P. Huntington, Opt. Commun. **134,** 66 (1997).
22. T. X. Phuoc, Opt. Commun. **175,** 419 (2000).
23. J. P. Davis, A. L. Smith, C. Giranda, and M. Squicciarini, Appl. Opt. **30,** 4358 (1991).
24. D. I. Rosen and G. Weyl, J. Phys. D **20,** 1264 (1987).
25. A. Sircar, R. K. Dwivedi, and R. K. Thareja, Appl. Phys. B **63,** 623 (1996).
26. S. Yalcin, D. R. Crosley, G. P. Smith, and G. W. Faris, Appl. Phys. B **68,** 121 (1999).
27. A. Vogel, K. Nahen, D. Theisen, R. Birngruber, R. J. Thomas, and B. A. Rockwell, Appl. Opt. **38,** 3636 (1999).
28. L. R. Evan and C. G. Morgan, Phys. Rev. Lett. **22,** 1099 (1969).
29. Z.-O. D. Program, 10.0 ed. (Focus Software Inc.).
30. S. S. Harilal, C. V. Bindhu, M. S. Tillack, F. Najmabadi, and A. C. Gaeris, J. Phys. D **35,** 2935 (2002).
31. S. S. Harilal, C. V. Bindhu, M. S. Tillack, F. Najmabadi, and A. C. Gaeris, J. Appl. Phys. **93,** 2380 (2003).
32. L. J. Radziemski and D. A. Cremers, *Laser Induced Plasmas and Applications* (Marcel Dekker, New York, 1989).
33. M. Longenecker, L. Huwel, L. Cadwell, and D. Nassif, Appl. Opt. **42,** 990 (2003).
34. T. A. Spiglanin, A. McIlroy, E. W. Fournier, R. B. Cohen, and J. A. Syage, Combust. Flame **102,** 310 (1995).
35. S. S. Harilal, C. V. Bindhu, V. P. N. Nampoori, and C. P. G. Vallabhan, Appl. Spectrosc. **52,** 449 (1998).
36. H. R. Griem, *Principles of Plasma Spectroscopy* (Cambridge, New York, 1997).
37. http://physics.nist.gov.
38. H. R. Griem, *Plasma Spectroscopy* (McGraw-Hill, New York, 1964).
39. Y. B. Zeldovich and Y. P. Raizer, *Physics of Shock Waves and High-Temperature Hydrodynmaic Phenomena* (Dover Publications, Inc., New York, 2002).
40. J. J. Chang and B. E. Warner, Appl. Phys. Lett. **69,** 473 (1996).
41. S. S. Harilal, C. V. Bindhu, R. C. Issac, V. P. N. Nampoori, and C. P. G. Vallabhan, J. Appl. Phys. **82,** 2140 (1997).
42. R. K. Singh and J. Narayan, Phys. Rev. B **41,** 8843 (1990).